Accepted to Phys. Fluids 10.1063/5.0154768

A new elastic instability in gravity-driven viscoelastic film flow

Mamta Priyadarshi,[1, a)] Kopparthi V. Srita,[1, a)] V. V. K. N. Sai Bhaskar,[1] Mohammad Khalid,[1] Ganesh Subramanian,[2, b)] and V. Shankar[1, c)]

[1)]*Department of Chemical Engineering, Indian Institute of Technology, Kanpur 208016, India*

[2)]*Engineering Mechanics Unit, Jawaharlal Nehru Center for Advanced Scientific Research, Bangalore 560084, India*

Accepted to Phys. Fluids 10.1063/5.0154768

We examine the linear stability of the gravity-driven flow of a viscoelastic fluid film down an inclined plane. The viscoelastic fluid is modeled using the Oldroyd-B constitutive equation, and therefore, exhibits a constant shear viscosity and a positive first normal stress difference in viscometric shearing flows; the latter class of flows includes the aforesaid film-flow configuration. We show that the film-flow configuration is susceptible to two distinct purely elastic instabilities in the inertialess limit. The first instability owes its origin entirely to the existence of a free surface and has been examined earlier (Shaqfeh *et al.*, Journal of non-Newtonian Fluid Mehcanics, **31**, 87-113, (1989)). The second one is the analog of the centermode instability recently discovered in plane Poiseuille flow (Khalid *et al.*, Physical Review Letters, **127**, 134502 (2021)) and owes its origin to the base-state shear; it is an example of a purely elastic instability of shearing flows with rectilinear streamlines.

One may draw an analogy of the aforesaid pair of unstable elastic modes with the inertial free-surface and shear-driven instabilities known for the analogous flow configuration of a Newtonian fluid. While surface tension has the expected stabilizing effect on the Newtonian and elastic free-surface modes, its effect on the corresponding shear modes is, surprisingly, more complicated. For both the Newtonian shear mode and the elastic centermode, surface tension plays a dual role, with there being parameter regimes where it acts as a stabilizing and destabilizing influence. While the Newtonian shear mode remains unstable in the limit of vanishing surface tension, the elastic centermode becomes unstable only when the appropriate non-dimensional surface tension parameter exceeds a threshold. In the limit of surface tension being infinitely dominant, the free-surface boundary conditions for the film-flow configuration reduce to the centerline symmetry conditions satisfied by the elastic centermode in plane Poiseuille flow. As a result, the regime of instability of the film-flow centermode becomes identical to that of the original channel-flow centermode. At intermediate values of the surface tension parameter, however, there exist regimes where the film-flow centermode is unstable even when its channel-flow counterpart is stable. We end with a discussion of the added role of inertia on the aforementioned elastic instabilities.

[a)]These authors contributed equally to this work.
[b)] Author for correspondence; E-mail: sganesh@jncasr.ac.in
[c)] Author for correspondence; E-mail: vshankar@iitk.ac.in

Accepted to Phys. Fluids 10.1063/5.0154768

I. INTRODUCTION

Understanding the stability and dynamics of liquid films flowing over a surface has important implications in coating-flow processes such as slide delivery[1], wherein single or multiple liquid layers are made to flow on an inclined surface prior to their application onto a web. Such gravity-driven film flows are prone to instabilities that could be detrimental to the coating process by causing nonuniformities in the coated film. While the instability may be driven by the free surface for a single liquid film, for multiple liquid layers, each of the internal liquid-liquid interfaces is also potentially susceptible to instabilities that, for Newtonian liquids, arise due to a jump in viscosity or density[2–5], and require inertia. However, in many coating applications, the liquids being coated are rheologically complex, and often viscoelastic, due to the presence of polymer additives in the formulation. Viscoelastic film-flow configurations involving a single liquid layer with a free surface, or multiple liquid layers with internal interfaces, are again prone to instabilities, with the instability of the multi-layer configurations now arising from the interfacial jump of an elastic property: most often, the first normal stress difference[6–8] which leads to growing perturbations along the direction of the flow; and less frequently, due to the smaller second normal stress difference which leads to the growth of spanwise varying perturbations[9]. Importantly, in contrast to the Newtonian case, such normal-stress-driven interfacial instabilities occur even in the absence of inertia.

In addition to the interfacial instabilities mentioned above, one may have competing effects arising from bulk instabilities. For Newtonian liquids, bulk instabilities arise from the shear within the flowing film, requiring only inertia or the combined influence of inertia and viscosity. In contrast, it is now well known, based on research in the last three and a half decades, that viscoelastic fluids can sustain purely elastic bulk instabilities even in the inertialess limit[10–12]. Examples of such elastic instabilities include those that occur in the canonical rheometric configurations, for instance, the cone-and-plate, parallel-disc, and Taylor-Couette geometries. Importantly, unlike the viscoelastic interfacial instabilities, all of the above bulk elastic instabilities pertain to curvilinear shearing flows. Thus, the growth of infinitesimal amplitude perturbations in all cases is driven by hoop stresses that arise due to the tension along the curved base-state streamlines, with the tension itself being the result of a positive first normal stress difference[11,13].

In the present study, we revisit the stability of gravity-driven viscoelastic film flow over an inclined plane surface (termed the single-layer configuration above), a configuration previously

considered by Gupta[14], Lai[15], and Shaqfeh *et al.*[16], with an objective of characterizing all possible unstable modes in this flow configuration. The said studies were motivated, in part, by the classical analyses of Benjamin[2] and Yih[3] which first showed that gravity-driven Newtonian film-flow is prone to a long-wave surface instability, termed the free-surface mode herein (and abbreviated FSM henceforth), with a threshold Reynolds number that is a function of the angle of inclination. The studies of Gupta[14], Lai[15], and Shaqfeh *et al.*[16] have shown that, much like the scenario for the bulk instabilities discussed in the previous paragraph, the viscoelastic analog of the above film-flow configuration is susceptible to a long-wave elastic instability even in the absence of inertia; we refer to this as the 'elastic FSM' to, on one hand, distinguish it from the aforesaid (Newtonian) FSM, and on the other hand, to emphasize the existence of a free surface as being essential for its existence. Now, in the Newtonian case, as first shown by Lin[17] and later, in a more comprehensive investigation by Floryan and co-workers[18], there also exists a competing bulk-shear-driven mode that governs the transition from the unidirectional base-state for very small angles of inclination (less than about $0.5^{\prime}$); this change from an FSM-controlled transition to a shear-mode-controlled one occurs because the FSM threshold diverges in the limit of a horizontal surface. A natural question to ask is if there exists a similar (elastic) bulk-shear mode for the viscoelastic film-flow configuration that likewise controls the transition for sufficiently shallow inclinations.

Until recently, the answer to the question above would have been in the negative. As already mentioned above, all of the known linear elastic instabilities, driven by a bulk shear, are also known to require streamline curvature, and would appear to be absent for gravity-driven flow over any plane surface, in turn implying that the analyses of Gupta[14], Lai[15] and Shaqfeh *et al.*[19] are complete. However, research in the last five years which includes experiments[20,21], linear stability analyses[22–26], computations of exact nonlinear traveling wave structures[27,28], and direct numerical simulations[29], has shown that novel elastoinertial, and even purely elastic, instabilities can arise in rectilinear shearing flows devoid of a base-state streamline curvature[30]. In particular, the existence of a linear purely elastic instability for a rectilinear shearing flow was first shown by Khalid *et al.*[30], for the case of plane Poiseuille (channel) flow, by the explicit calculation of an unstable eigenfunction and the associated growth rate, using both spectral and shooting formulations. In light of the aforementioned very recent research, one expects the stability scenario for gravity-driven viscoelastic film flow to be similar to its Newtonian counterpart, in the sense of supporting both free-surface-driven and bulk-shear-driven elastic modes in the absence of inertia, and estab-

lishing this fact is indeed one of the primary motivations of the present effort. We show that there do exist two qualitatively different elastic instabilities of the viscoelastic film-flow configuration: the long-wave elastic FSM predicted in the earlier efforts highlighted above[14–16], and the analog of the finite-wavelength elastic centermode (CM) instability for channel flow[30] which has a lower threshold for sufficiently small angles of inclination.

It is useful to discuss, at the outset, the rationale for anticipating an analog of the aforesaid elastic CM in the present film-flow configuration. While the base-state for gravity-driven flow of an Oldroyd-B fluid film is the half plane-Poiseuille profile, the eigenfunctions are required to satisfy the kinematic, normal stress, and tangential stress conditions at the free surface instead. The latter is in contrast to channel flow where the eigenfunctions satisfy no-slip conditions at the rigid boundaries. Thus, the unstable eigenfunctions in the two configurations are expected to be different in general. In the limit of surface tension going to infinity, however, the free-surface conditions reduce to symmetry conditions at the channel centerline, and the film-flow eigenmode therefore reduces to the original channel-flow CM eigenfunction (restricted to the half-channel domain)[30]. Interestingly, in the original Newtonian case, the eigenfunction for the bulk shear instability in channel flow (the well-known Tollmein-Schlichting (TS) mode) is antisymmetric, with a nonzero wall-normal velocity at the channel centerline. Since free-surface fluctuations become negligible for an infinite surface tension, the resulting incompatibility with a finite wall-normal velcoity implies that the bulk shear instability is absent in this taut interface limit. In the opposite so-called floppy-interface limit, the amplitude of the free surface fluctuations remains finite, and hence, it is permissible to have a non-zero wall-normal velocity, consistent with antisymmetry of the TS eigenfunction. Despite this, there is no direct connection between the shear-driven mode in the film-flow configuration, and the channel flow TS mode, owing to the additional shear-stress boundary condition in the former case. Such a connection was erroneously postulated in the early eff ort of Lin (1967)[17], with the error being clarified in the later effort of Floryan *et al.* (1987)[18].

Before moving on to the organization of the manuscript, we briefly mention more recent efforts that have addressed the influence of additional physical factors on the elastic FSM above. The efforts of Wei[31] and Pal and Samanta[32,33] have examined the effects of imposed shear, wall slip, as well as the presence of surfactants on the free-surface instability in viscoelastic film flows. The effort of Hu *et al.*[34] has studied the nonlinear evolution of the viscoelastic film-flow configuration using a reduced model, and in the limit of weak elasticity, predicts the formation of steady permanent waves for long times. Although not directly relevant to the present problem, several recent

Accepted to Phys. Fluids 10.1063/5.0154768

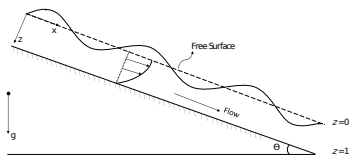

FIG. 1. Schematic of the configuration: a viscoelastic liquid film flowing down an inclined surface.

efforts have examined the evolution of viscoelastic films on a wavy surface.

The remainder of this paper is organized as follows: Section II provides the governing equations and boundary conditions, along with the linearized system of equations, within a temporal stability framework, that govern the stability to imposed small-amplitude perturbations. Section III provides a discussion of the results of the linear stability analysis. We first examine the inertialess limit in section III A, before going on to describe the role of finite inertia in section III B. The salient conclusions of this study are provided in Section IV.

II. PROBLEM FORMULATION

We consider the gravity-driven flow of an incompressible viscoelastic liquid layer down an inclined plane which makes an angle θ with the horizontal (Fig. 1). The viscoelastic liquid is modeled using the Oldroyd-B constitutive relation[35,36], in which the total stress is given by the sum of Newtonian solvent and viscoelastic polymeric contributions. The model has three material constants: the shear-rate-independent polymer contribution to the viscosity μ_p, the polymer relaxation time λ, and the solvent viscosity μ_s; the solution viscosity being given by $\mu = \mu_p + \mu_s$. As will be seen below, these three dimensional parameters lead to a pair of non-dimensional parameters - the Weissenberg number and the solvent-to-solution viscosity ratio - that, among others, govern the instability threshold. The aforesaid liquid layer (film) of density ρ has a uniform thickness in the base state, occupying the region $0 < z^* < H$, and is assumed to be in contact with a passive gas that has a negligible viscosity, and is therefore accounted for via a free-surface boundary condition[37]. In the equations given below, the following scales are used to nondimensionalize various quantities: lengths by the base-state film thickness H, velocities by the speed at the free-surface of the

unperturbed liquid layer $V \equiv \frac{\rho g H^2 \sin\theta}{2\mu}$, time by $\frac{H}{V}$, pressure by $\frac{\mu V}{H}$, polymeric stresses by $\frac{\mu_p V}{H}$, and solvent stresses by $\frac{\mu_s V}{H}$.

A. Governing equations

The dimensionless equations governing the dynamics of the liquid layer are the mass conservation and Cauchy momentum equations:

$$\boldsymbol{\nabla}\cdot\mathbf{v} = 0, \tag{1}$$

$$Re\left[\frac{\partial \mathbf{v}}{\partial t} + \mathbf{v}\cdot\boldsymbol{\nabla}\mathbf{v}\right] = \boldsymbol{\nabla}\cdot\mathbf{T} + \frac{2}{\sin\theta}\hat{\mathbf{g}}. \tag{2}$$

Here, $\mathbf{v}$ is the velocity field in the liquid, $\hat{\mathbf{g}}$ is the unit vector pointing in the direction of gravity and $Re = \rho V H/\mu$ is the Reynolds number. The total stress tensor in the fluid, $\mathbf{T} = -p\mathbf{I} + \boldsymbol{\tau}$, is the sum of an isotropic pressure and an extra stress tensor $\boldsymbol{\tau} = \beta\boldsymbol{\tau}^s + (1-\beta)\boldsymbol{\tau}^p$, with $\beta = \frac{\mu_s}{\mu}$ being the ratio of the solvent and solution viscosities. The Newtonian solvent contribution to $\boldsymbol{\tau}$ is given by $\boldsymbol{\tau}^s = [\boldsymbol{\nabla}\mathbf{v} + (\boldsymbol{\nabla}\mathbf{v})^T]$, while $\boldsymbol{\tau}^p$, the polymeric contribution to $\boldsymbol{\tau}$, is governed by the Oldroyd-B constitutive relation[35,36]:

$$W\left[\frac{\partial \boldsymbol{\tau}^p}{\partial t} + \mathbf{v}\cdot\boldsymbol{\nabla}\boldsymbol{\tau}^p - (\boldsymbol{\nabla}\mathbf{v})^T\cdot\boldsymbol{\tau}^p - \boldsymbol{\tau}^p\cdot\boldsymbol{\nabla}\mathbf{v}\right] + \boldsymbol{\tau}^p = \boldsymbol{\nabla}\mathbf{v} + (\boldsymbol{\nabla}\mathbf{v})^T. \tag{3}$$

Here, $W \equiv \frac{\lambda V}{R}$ is the Weissenberg number that is the ratio of the polymer relaxation time to a characteristic flow time scale, and thereby, a non-dimensional measure of the fluid elasticity. In the limit $\beta = 0$, the Oldroyd-B model reduces to the upper-convected Maxwell (UCM) model which provides an approximate description of the rheology of polymer melts. Either of the limits $W = 0$ and $\beta = 1$ correspond to that of a Newtonian fluid.

The boundary conditions at the free surface include a dynamic component that involves the tangential and normal stress balances, and a kinematic component that involves the velocity normal to the evolving free surface. Because the overlying gas is assumed to be passive, the tangential stress balance reduces to the tangential stress at the free surface of the liquid layer being zero, with the normal stress equalling a constant hydrostatic pressure plus surface tension times curvature of the perturbed free surface. The kinematic and dynamic boundary conditions may therefore be

written in the form:

$$\partial_t h + v_x \partial_x h = v_z, \tag{4}$$

$$\mathbf{n}\cdot\mathbf{T}\cdot\mathbf{t} = 0, \tag{5}$$

$$\mathbf{n}\cdot\mathbf{T}\cdot\mathbf{n} = \Sigma(\boldsymbol{\nabla}\cdot\mathbf{n}), \tag{6}$$

where $h(x,t)$ describes the free surface position for perturbations uniform along the spanwise (y) direction, while $\mathbf{n}$ and $\mathbf{t}$ are the unit normal (pointing out of the liquid layer) and unit tangent vectors to the free surface, respectively. Note that the boundary conditions (5) and (6) are stated in invariant form, and are thereby valid for an arbitrarily deformed free surface; $\mathbf{t} = \mathbf{1_x}$ and $\mathbf{n} = -\mathbf{1_z}$ for the uniform layer in the base-state. The normal stress boundary condition (6) includes a dimensionless surface tension parameter $\Sigma = \gamma/(\mu V)$, with γ being the coefficient of surface tension; Σ is the inverse of the capillary number $Ca = \mu V/\gamma$. Other dimensionless measures of surface tension have also been suggested in the literature: the Ohnesorge number $Oh = (Ca/Re)^{1/2}$, the elastic capillary number W/Ca, and the Weber number $We = ReCa$, the former two being independent of the flow velocity scale[12].

B. Base State

The laminar base state whose stability is examined here is the gravity-driven flow of a non-shear-thinning elastic liquid, in the x direction, with an undeformed plane free surface. The non-dimensional velocity, pressure and polymeric stress fields for this base state (represented by an overbar) are given by:

$$\overline{v}_x = 1 - z^2, \qquad \overline{v}_z = 0, \tag{7}$$

$$\overline{p} = 2z\cot\theta, \qquad \overline{\tau}^p_{zz} = 0, \tag{8}$$

$$\overline{\tau}^p_{xz} = -2z, \qquad \overline{\tau}^p_{xx} = 8Wz^2. \tag{9}$$

The positive $\overline{\tau}^p_{xx}$ characterizes the tension along the rectilinear base-state streamlines arising from stretched polymer molecules. This tension is a quadratic function of the transverse coordinate (z), but is zero at the free surface ($z = 0$) owing to the base-state shear vanishing at this location.

C. Linearized governing equations

A temporal linear stability analysis is performed wherein all dynamical quantities are perturbed about the base state defined in section II B above, and substituted in the governing equations, with only terms linear in the perturbations being retained. At linear order, the perturbation f' to any physical variable may be expanded in terms of independent non-interacting Fourier modes of the form:

$$f' = \tilde{f}(z)\exp[ik(x-ct)]\,, \tag{10}$$

where k is the (real) wave number of the Fourier mode, $c = c_r + ic_i$ the complex wavespeed, and $\tilde{f}(z)$ the complex amplitude function that governs the 'shape' of the disturbance. The flow is unstable (stable) if $c_i > 0$ (< 0) for one or more Fourier modes. When the above ansatz is used in the linearized equations and boundary conditions, one obtains a set of linear ODEs that governs the z-dependence of the amplitude functions, and that involves the wavespeed c. The system of ODEs governing the evolution of small amplitude perturbations to the gravity-driven viscoelastic film flow configuration are given by:

$$\mathrm{d}_z\tilde{v}_z + ik\tilde{v}_x = 0\,, \tag{11}$$

$$\begin{aligned} Re\,[ik(\bar{v}_x - c)\tilde{v}_x + (\mathrm{d}_z\bar{v}_x)\tilde{v}_z] = &-ik\tilde{p} + \beta[\mathrm{d}_z^2\tilde{v}_x - k^2\tilde{v}_x] \\ &+(1-\beta)[ik\tilde{\tau}^p_{xx} + \mathrm{d}_z\tilde{\tau}^p_{xz}], \end{aligned} \tag{12}$$

$$\begin{aligned} Re\,[ik(\bar{v}_x - c)\tilde{v}_z] \;=\; &-\mathrm{d}_z\tilde{p} + \beta[\mathrm{d}_z^2\tilde{v}_z - k^2\tilde{v}_z] \\ &+(1-\beta)[ik\tilde{\tau}^p_{xz} + \mathrm{d}_z\tilde{\tau}^p_{zz}], \end{aligned} \tag{13}$$

with $\mathrm{d}_z \equiv \frac{d}{dz}$. The above equations can be combined to give a single fourth-order Orr-Sommerfeld-like equation for $\tilde{v}_z$:

$$\begin{aligned} ikRe[(\bar{v}_x - c)(\mathrm{d}_z^2 - k^2) - \mathrm{d}_z^2\bar{v}_x]\tilde{v}_z = &\beta(\mathrm{d}_z^2 - k^2)^2\tilde{v}_z + \\ &(1-\beta)[k^2\mathrm{d}_z(\tilde{\tau}^p_{xx} - \tilde{\tau}^p_{zz}) - ik(\mathrm{d}_z^2 + k^2)\tilde{\tau}^p_{xz}]\,, \end{aligned} \tag{14}$$

which reduces to the original Orr-Sommerfeld equation for $\beta = 1$. In (14), $\tilde{\tau}^p_{zz}$, $\tilde{\tau}^p_{xz}$ and $\tilde{\tau}^p_{xx}$ are obtained from the following linearized constitutive equations:

$$[1 + Wik(\bar{v}_x - c)]\tilde{\tau}^p_{zz} \;=\; 2(ikW\bar{\tau}^p_{xz}\tilde{v}_z + \mathrm{d}_z\tilde{v}_z), \tag{15}$$

$$[1+Wik(\bar{v}_x-c)]\tilde{\tau}^p_{xz} = W\mathrm{d}_z\bar{v}_x\tilde{\tau}^p_{zz}$$
$$-[W\mathrm{d}_z\bar{\tau}^p_{xz} - ik(1+W\bar{\tau}^p_{xx})]\tilde{v}_z + \mathrm{d}_z\tilde{v}_x, \tag{16}$$

$$[1+Wik(\bar{v}_x-c)]\tilde{\tau}^p_{xx} = 2W\mathrm{d}_z\bar{v}_x\tilde{\tau}^p_{xz} -$$
$$W\mathrm{d}_z\bar{\tau}^p_{xx}\tilde{v}_z + [2ik(1+W\bar{\tau}^p_{xx})]\tilde{v}_x + 2W\bar{\tau}^p_{xz}\mathrm{d}_z\tilde{v}_x\,. \tag{17}$$

The linearized kinematic, and tangential, and normal stress boundary conditions at the unperturbed free surface ($z=0$) are:

$$ik[\bar{v}_x-c]\tilde{h} = \tilde{v}_z\,, \tag{18}$$
$$\beta[-2\tilde{h} + (\frac{\mathrm{d}\tilde{v}_x}{\mathrm{d}z} + ik\tilde{v}_z)] + (1-\beta)[\tilde{\tau}^p_{xz} + \frac{\mathrm{d}\bar{\tau}^p_{xz}}{\mathrm{d}z}\tilde{h}] = 0, \tag{19}$$
$$-\tilde{p} - (2\,cot\theta)\tilde{h} - k^2\Sigma\tilde{h} + 2\beta\,\frac{\mathrm{d}\tilde{v}_z}{\mathrm{d}z} + (1-\beta)\tilde{\tau}^p_{zz} = 0\,. \tag{20}$$

The boundary conditions at the underlying rigid surface ($z=1$) are the usual no-slip conditions for $\tilde{v}_z$ and $\tilde{v}_x$.

The above system of linear ODEs and boundary conditions constitute an eigenvalue problem for the complex wavespeed c as a function of the non-dimensional parameters Re, W, β, k, θ and Σ. To solve for c, we have employed two different numerical methods; the first being a Chebyshev spectral collocation method which gives the complete spectrum of eigenvalues for specified values of the aforementioned non-dimensional parameters, including both the discrete spectra and discretized versions of the continuous spectra; the second being a~~n orthonormal~~ numerical shooting procedure[38], combined with a Newton-Raphson method, that solves the characteristic equation for the eigenvalue c starting from an appropriate initial guess. Owing to the high-dimensional parameter space, the results presented below pertain to a pair of inclination angles: $\theta = 50^\circ$ and $\theta = 90^\circ$, the latter corresponding to a vertical-film configuration that is the most unstable.

III. RESULTS AND DISCUSSION

To begin with, it is worth emphasizing a novel feature of the present investigation - the identification of *two* elastic instabilities, of distinct physical origins, associated with a given shearing flow configuration. This is in contrast to almost all earlier research on purely elastic instabilities in viscometric shearing flows as summarized, for instance, in Larson (1992) or Shaqfeh (1996). In cases where the shearing flow is entirely bounded by rigid surfaces, examples of which include

the Taylor-Couette[39] and Taylor-Dean configurations[40], or the torsional flow in the parallel-plate[41] or cone-and-plate[42] geometries, the purely elastic instability identified in earlier efforts invariably owes its origin to hoop stresses associated, directly or indirectly, with the curvature of the base-flow streamlines. That the base-state streamline curvature is the underlying cause of all of the above elastic instabilities is reinforced by the so-called Pakdel-Mckinley criterion[43].

For the gravity-driven film-flow configuration examined here, the earlier efforts of Gupta[14] and Shaqfeh, Larson, and Fredrickson[16] have established the existence of a long-wavelength purely elastic instability whose origin is intimately linked to the presence of a free surface, and is henceforth referred to as the free-surface mode ('FSM'). A hallmark of this unstable mode is that its phase speed, in the long-wave limit ($k \to 0$), is twice the base-state maximum (that occurs at the free surface), a relation that arises from the volumetric flow rate per unit span scaling as the square of the liquid layer thickness[2]. Herein, we show that, in addition to this mode, the film flow configuration supports a second *finite-wavelength* elastic instability with phase speed approximately equal to the base-state maximum. This latter mode is shown to be an analog of the unstable 'centermode' originally identified in both viscoelastic pipe[22,24] and plane[25] Poiseuille flow in presence of inertia, and more recently, extended to the inertialess limit for the plane Poiseuille flow case[30]. The latter extension led to the discovery of an elastic instability of shearing flows with rectilinear streamlines that arises from a novel critical-layer mechanism[30] as opposed to the aforementioned hoop-stress origin of the usual elastic instabilities. For plane Poiseuille flow, the said unstable mode has a phase speed nearly equal to the base-state maximum which occurs at the channel centerline, and hence the aforementioned terminology of a centermode. While the centermode nomenclature is natural for the channel flow geometry, we continue to use this terminology for the finite-wavelength unstable mode discovered here, for the film-flow configuration, since, as mentioned above, the mode continues to have a phase-speed close to the base-state maximum; the identity of the film-flow and channel centermodes, for $\Sigma \to \infty$, was discussed in the introduction. Further, it was shown Khalid *et. al*[30] that, for plane Poiseuille flow, the elastic centermode instability occurs only when $\beta \gtrsim 0.99$, and accordingly, we focus on this ultra-dilute regime in the present study.

In light of the above discussion, the results below are organized into two parts: an initial longer description focused on the inertialess limit ($Re = 0$), followed by a shorter exploration of the added influence of fluid inertia ($Re \neq 0$) on the growth rates and domains of existence of the two unstable modes. While all of the detailed results with regard to the eigenspectra, the growth rate and phase

speed variations, etc, presented below, pertain to $\theta = 50^\circ$, the neutral stability envelopes are given for both $\theta = 50^\circ$ and $\theta = 90^\circ$.

A. The inertialess limit: $Re = 0$

Figure 2 shows the eigenspectrum in the absence of surface tension ($\Sigma = 0$) for $\beta = 0.995$, $W = 900$ and $k = 1$. A well-known feature of the eigenspectra for viscoelastic shear flows is the presence of an elastic continuous spectrum (abbreviated 'CS' henceforth) that owes its origin to the spatially local nature of the Oldroyd-B equation, and comprises eigenvalues with real parts (phase speeds) that vary continuously in the base range of velocities, and with $c_i = -1/(kW)$ corresponding to decay rates that equal the inverse relaxation time[23]. The theoretical CS is a branch cut in the complex c-plane[44], and allows for eigenvalues to disappear into and/or reappear from it with changes in one or more parameters (such as W as discussed below; also see[24,25]). For any $\beta \neq 1$, there is also a second viscous continuous spectrum[23,44] with $c_i = -1/(\beta kW)$, although, for the ultra-dilute regime ($\beta \to 1$) under consideration, the decay rates of these viscous CS-modes are practically indistinguishable from those belonging to the elastic CS.

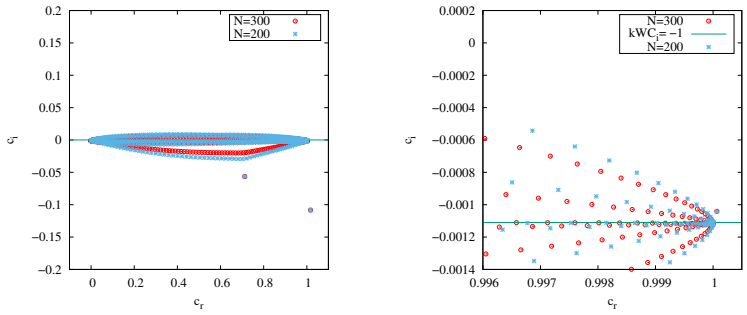

(a) Overall features of the spectrum (b) Enlarged view of spectrum near $c_r = 1$

FIG. 2. Elastic eigenspectrum for film flow of an Oldroyd-B fluid, demonstrating the presence of a stable (discrete) centermode with $c_r \approx 1$, just above and to the right of the CS balloon; $\Sigma = 0$, $\beta = 0.995$, $W = 900$, $k = 1$, $Re = 0$, $\theta = 50^\circ$.

The aforementioned CS is present in the numerically computed elastic eigenspectrum in Fig 2a, albeit as a ballooned-up structure around the theoretically predicted horizontal segment ($0 < c_r < 1; c_i = -1/(kW)$) owing to the finite numerical resolution; the balloon does narrow down with

Accepted to Phys. Fluids 10.1063/5.0154768

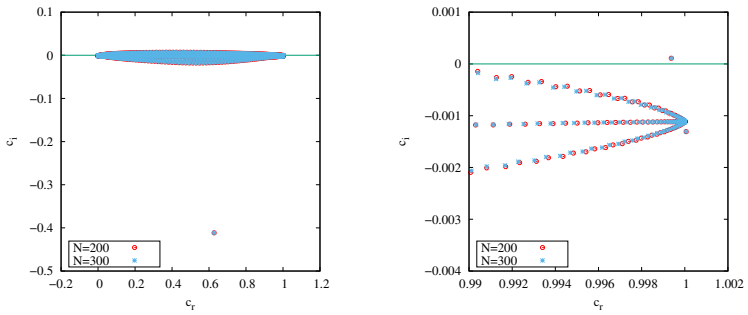

(a) Overall features of the spectrum (b) Enlarged view of spectrum near $c_r = 1$

FIG. 3. Elastic eigenspectrum for film flow of an Oldroyd-B fluid, demonstrating the presence of an unstable centermode for $\Sigma = 80$. Other parameters are identical to Fig 2: $\beta = 0.995$, $W = 900$, $k = 1$, $Re = 0$, $\theta = 50°$.

increase in the number of collocation points (from $N = 200$ to 300). The magnified view of the neighborhood of $c_r = 1$ in Fig 2b shows that, in addition to the CS, there is also a stable discrete mode just above and to the right of the CS balloon which, for reasons mentioned earlier, we label as the 'centermode'[45]. Further, as shown in Fig 3, this centermode becomes unstable as Σ is increased to 80, with other parameters remaining fixed. This transition of the centermode to instability occurs for $k \sim O(1)$, and is therefore in stark contrast to the FSM analyzed by Gupta[14] and Shaqfeh *et al.*[16]. For the ultra-dilute regime under consideration, the latter mode is unstable only for $k \ll 1$, rendering it much less significant than its Newtonian counterpart[2,3].

A noteworthy feature is the dual role of surface tension on the elastic CM identified above. While Figs. 2 and 3 showed that increasing surface tension (from $\Sigma = 0$ to 80) leads to a destabilization of the centermode, Fig 4 shows that the resulting instability persists only over a finite range of Σ values, with the CM again becoming stable for sufficiently high Σ. It is therefore useful to speculate on the reasons that underlie the non-monotonic variation of the growth rate, with increasing Σ, in Fig. 4b; we present arguments in this regard in the limits $\Sigma = 0$ and $\Sigma \to \infty$. To begin with, note that the elastic CM identified previously in the channel-flow configuration is a symmetric mode[25,30], the symmetry pertaining to that of the tangential velocity eigenfunction about the channel centerline, and as a result, the wall-normal perturbation velocity is identically zero at the centerline. In light of this, one expects the elastic CM to be carried over from the channel-flow to the film-flow configuration, provided the free surface remains undeformed (or nearly so).

Accepted to Phys. Fluids 10.1063/5.0154768

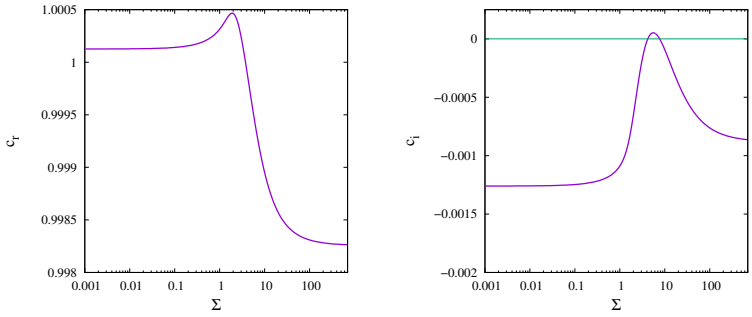

(a) c_r vs Σ (b) c_i vs Σ

FIG. 4. The dual role of surface tension on the elastic centermode, illustrated via the variation of c_r and c_i as a function of Σ; $\beta = 0.995$, $W = 480$ and $k = 1.5, Re = 0$, $\theta = 50^\circ$.

Examining the 'floppy-interface' limit ($\Sigma = 0$) first, one finds the aforementioned constraint of an undeformed free surface to be in conflict with the non-trivial variation of the elastic CM polymeric normal stresses along the channel centerline ($\tilde{\tau}^p_{zz}\,|_{z=0}$) that would necessarily perturb the free surface. In other words, the original CM eigenfunction fails to satisfy the normal stress boundary condition, (Eq. 20), thereby precluding a direct connection, for $\Sigma \ll 1$, between the elastic CM identified above and that for channel flow. Not surprisingly therefore, the CM for the film-flow configuration remains stable for $\Sigma \to 0$.

In the opposite 'taut-interface' limit ($\Sigma \to \infty$), as alluded to in the Introduction, the normal stress boundary condition (Eq. 20) shows that the free surface perturbation $\tilde{h}$ must be $O(\Sigma^{-1})$, and hence, vanishingly small. Assuming, therefore, an unperturbed interface for $\Sigma \to \infty$, the kinematic boundary condition, Eq. 18, implies a zero normal velocity component ($\tilde{v}_z = 0$). Further, Eq. 20 is satisfied provided the polymeric shear stress ($\tilde{\tau}^p_{xz}$) is zero, and the tangential velocity component has a zero slope ($d\tilde{v}_x/dz = 0$) at the unperturbed free surface, both of which are true for the channel-flow CM. This implies that the original channel-flow CM eigenfunction, now restricted to the half-channel domain, satisfies both the kinematic and shear stress boundary conditions at the free surface in the limit $\Sigma \to \infty$. Note that the only constraint arising from the normal stress boundary condition is the requirement of an unperturbed free surface, as already mentioned above; the combination $\Sigma\tilde{h}$ remains non-trivial for $\Sigma \to \infty$, allowing the unperturbed interface to nevertheless support an arbitrary jump in normal stresses. The implication of the above arguments is

Accepted to Phys. Fluids 10.1063/5.0154768

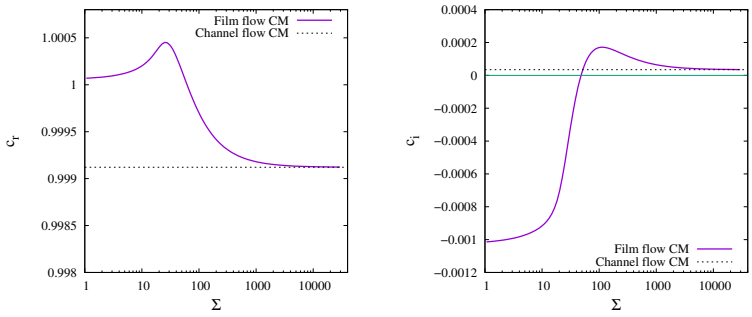

(a) c_r vs Σ (b) c_i vs Σ

FIG. 5. Figure illustrating the elastic centermode being unstable even in the $\Sigma \gg 1$ limit. The dotted horizontal line shows the eigenvalue obtained from channel flow for the same set of parameters. Data for $\beta = 0.995, W = 1150$ and $k = 0.8, Re = 0$, $\theta = 50^\circ$.

that the elastic CM for the film-flow configuration approaches the original elastic CM in the limit $\Sigma \to \infty$. For the particular choice of parameters in Fig. 4, however, the latter is stable, and it is this that causes the stabilization of the film-flow CM for sufficiently large Σ. To reinforce the above inference, in Fig. 5, we show the variation of c_r and c_i with Σ at a much higher $W = 1150$, and for $k = 0.8$, which correspond to the channel-flow CM being unstable. While we again find surface tension to play an initial destabilizing role similar to Fig. 4, the elastic CM now remains unstable in the limit of $\Sigma \to \infty$. A noteworthy feature in both Figs. 4 and 5 is that the magnitude of c_i is highest for an intermediate finite Σ ($\Sigma \sim O(1)$ in Fig. 4, and $\Sigma \sim O(100)$ in Fig. 5), suggesting that the film flow configuration is more unstable than its channel-flow counterpart, with the elastic CM for the former remaining unstable even in parameter regimes (in the $W - k$ plane) where the original channel-flow CM is stable.

On the whole, the role of surface tension described above remains counterintuitive. While surface tension is known to play a destabilizing role for liquid jets/columns (the Rayleigh-Plateau instability), its effect in Figs. 4 and Fig. 5 does stand in contrast to its usual role for planar shearing flows where, most often, it solely acts to damp out large wavenumber fluctuations. This is essentially because the film-flow elastic CM, aside from relying on the bulk shear for destabilization, is associated with a nearly undeformed free surface for large Σ, rendering surface tension redundant.

One may ask the analogous question for the shear mode in the Newtonian film-flow problem.

Interestingly, and in contrast to the above, the TS-mode for Newtonian channel flow is antisymmetric, with a wall-normal velocity that remains finite at the channel centerline. Thus, for the TS-mode to be preserved in the film-flow configuration, the free surface must deform in a manner compatible with this normal velocity. For a vertical film ($\theta = 90^\circ$) in the floppy-interface limit, the resulting normal stress boundary condition may be shown to be identically satisfied by any antisymmetric eigenfunction (including the TS-mode in particular). A direct connection between the Newtonian channel and film-flow configurations is still absent, however, owing to the additional (zero) tangential stress boundary condition in the latter case. The threshold for the onset of the shear mode instability in the film-flow configuration therefore differs from the well-known threshold ($Re \approx 5772$) for linear instability in plane Poiseuille flow, being a function of the inclination angle[18]. As mentioned in the introduction, a connection between the Newtonian channel flow and film-flow problems, for $\Sigma = 0$, was erroneously attributed by Lin[17], although clarified in a later effort[18].

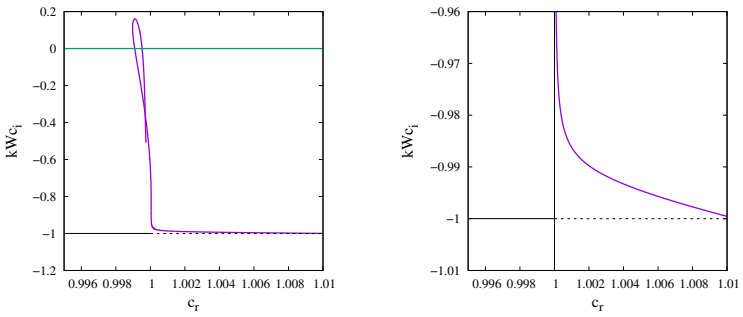

(a) kWc_i vs c_r (b) Enlarged region near $c_r = 1$

FIG. 6. The locus of the elastic centermode in the c_r–kWc_i plane, with changing k, for film flow of an Oldroyd-B fluid (k increases starting from the lower RHS corner). The horizontal black line represents the CS terminating at $c_r = 1$, its extension beyond this point being denoted by a dashed line. Data for $\beta = 0.995$, $W = 900$, $\Sigma = 80$, $Re = 0$, $\theta = 50^\circ$.

Figure 6 shows the locus of the centermode eigenvalue in the $c_r - kWc_i$ plane with changing k. The locus begins at the lower right corner for small k, moves to the left and then upward as k is increased, crossing the real axis (corresponding to a transition to instability), and then back (transition to stability), as $k \to \infty$. The pair of real-axis crossings imply that the elastic cen-

termode instability is present only over a rather small k-interval. While the absence of the centermode instability in the low-k limit is analogous to its absence in the floppy interface limit described above - it is the combination $k^2\Sigma$ that occurs in the normal stress boundary condition (20) - the stabilization at large k is somewhat counterintuitive, again along the lines of the large-Σ limit mentioned above. Note that even the original elastic centermode instability in plane Poiseuille flow[25,30] is only present over a finite range of k, for W fixed, an aspect that is preserved for the film-flow configuration. An intriguing feature in Fig 6a is that the eigenvalue locus appears to across the CS-line ($kWc_i = -1$) while remaining continuous, seemingly in violation of the fact that the CS is a branch cut in the complex c-plane. A closer examination in Fig 6b, however, reveals that the smooth variation occurs because $c_r > 1$ when $kWc_i = -1$, that is to say, the phase speed of the centerline is just outside the base range of velocities at the point that its decay rate equals those of the CS-modes, and there is therefore no crossing of the CS-line.

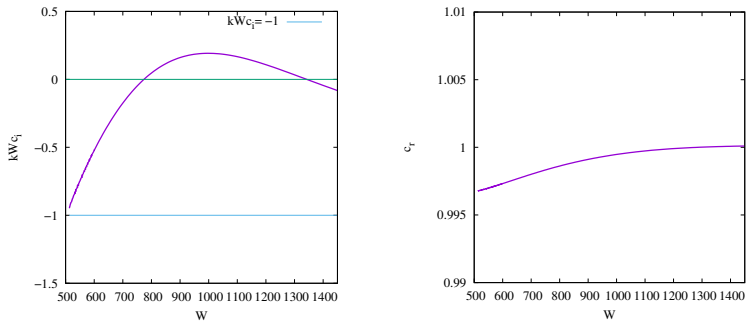

(a) kWc_i vs W (b) c_r vs W

FIG. 7. Emergence of the unstable mode from the CS as W is increased; $\beta = 0.995$, $k = 0.8$, $\Sigma = 80$, $Re = 0$, $\theta = 50^\circ$.

In Fig 7, we plot the variation of c_r and c_i with W in order to illustrate the origin of the elastic CM as W is increased. In Fig 7a, the CM is seen to first emerge from the CS at a threshold $W \approx 500$, move up towards the real axis, becoming unstable at $W \approx 771$, and transitioning back to stability at $W \approx 1343$; as shown in Fig 7b, c_r remains close to unity over the entire range of W examined. Similar to the k-dependence for a fixed W, the elastic centermode is unstable only over a finite range of W for a fixed k. Importantly, the absence of a CS in the Newtonian spectrum, associated with any shearing flow in a finite domain, ensures that the elastic centermode can have no Newtonian counterpart. In other words, one cannot smoothly continue the elastic centermode

onto any of the centermodes that populate the P-branch in the Newtonian spectrum. This behavior is identical to that found in an earlier more detailed examination of viscoelastic channel flow[25].

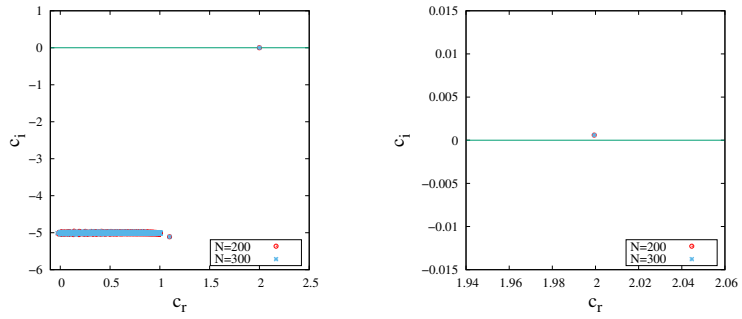

(a) Full eigenspectrum (b) Enlarged view near $c_r = 2$

FIG. 8. Eigenspectrum for Oldroyd-B film-flow showing the existence of an unstable free-surface mode (FSM) with $c_r \approx 2$; $\beta = 0.995$, $W = 200$, $k = 0.001$, $\Sigma = 80$, $Re = 0$, $\theta = 50^\circ$.

At this point, it is useful to briefly discuss features of the FSM, the second elastic instability present in the film-flow configuration, both in the interest of completeness and for purposes of comparison with features of the centermode instability discussed above. Fig 8 shows the elastic eigenspectrum for $k = 0.001$, and includes an unstable FSM; the small k value leads to the phase speed $c_r \approx 2$. Owing to the near-unity β, the FSM remains unstable only over a very small range of k, as seen in Fig 9. Fig 9a depicts the FSM eigenvalue locus on the complex c-plane; one moves along the locus starting from the lower left, as k decreases, eventually crossing the real axis, implying a transition to instability for sufficiently small k (see inset). Figure 9b shows c_r and c_i individually as functions of k. From the c_i-plot in this latter figure, one sees a transition to stability for $k \lesssim 0.002$. This renders the FSM, at least for $\beta \to 1$, less relevant in the sense of requiring an experimental system with an unrealistically large extent along the flow direction. This is perhaps the reason that the original linear stability analyses of Benjamin (1957) and Yih (1963) for the Newtonian surface mode have been followed up by a large number of efforts that account for the effects of nonlinearity (as reviewed in Chang (1994)[46], for instance), but that the earlier effort of Shaqfeh and co-workers (1989)[16] for the viscoelastic case has not attracted a similar level of attention.

Before proceeding to discuss the neutral stability curves for the FSM and CM, we illustrate, in

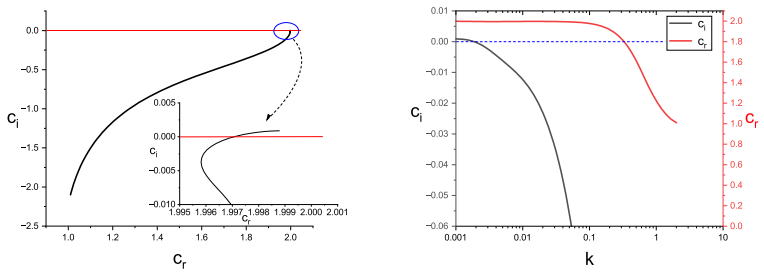

(a) c_r vs c_i (b) c_r and c_i vs. k

FIG. 9. (a) The locus of the FSM eigenvalue in the complex c-plane as k is increased from top right to bottom left; (b) Variation of c_r and c_i with k for the FSM. Data for $\Sigma = 5$, $\beta = 0.995$, $W = 300$, $Re = 0$, $\theta = 50^\circ$.

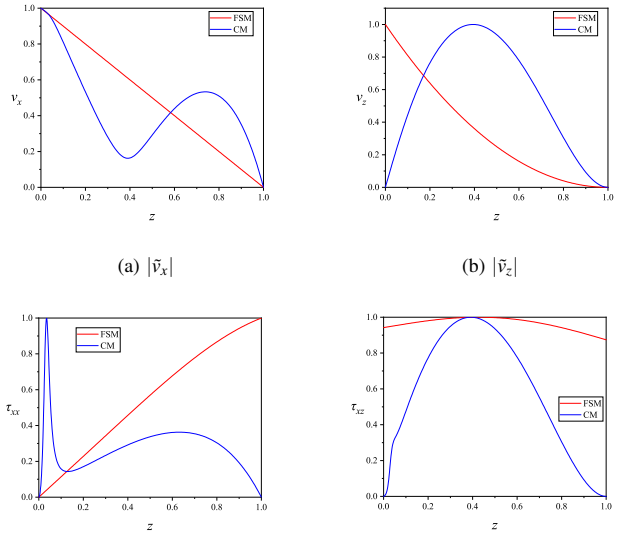

(a) $|\tilde{v}_x|$ (b) $|\tilde{v}_z|$

(c) $|\tilde{\tau}_{xx}|$ (d) $|\tilde{\tau}_{xz}|$

FIG. 10. Comparison of the velocity and stress eigenfunctions for the CM and FSM; data for $Re = 0$, $\beta = 0.995$, $\Sigma = 80$, and $\theta = 50^\circ$. The FSM eigenfunctions correspond to $W = 200$, $k = 0.001$, and to the eigenvalue $c = 1.99941 + 0.00059613\,i$. The CM eigenfunctions correspond to $W = 900$, $k = 1$, and to the eigenvalue $c = 0.999381 + 0.000111991\,i$.

Fig. 10, the qualitative differences between the respective eigenfunctions. The FSM eigenfunctions from the spectral code are shown for $k = 10^{-3}$, and for such low k, the numerical results agree very well with the analytical expressions from an asymptotic analysis[16,47] for the velocity and stress fields. In this limit, the streamwise velocity $\tilde{v}_x$ shows a linear variation, being driven by the shear stress at the perturbed free surface. Mass conservation then yields a normal velocity $\tilde{v}_z$ that is monotonic, exhibiting a quadratic variation with a maximum at the free surface and reaching zero at the bottom rigid wall. The above is in stark contrast to the $\tilde{v}_x$ and $\tilde{v}_z$ for the CM, both of which exhibit a non-monotonic variation with z. The $\tilde{\tau}_{xx}$ stress for the CM, in particular, shows a sharp peak close to the free surface, at a location termed the 'critical layer' where the phase speed c_r equals the local base-flow velocity. This feature is analogous to the elastic centermode in viscoelastic channel flow[30], and the aforesaid peak approaches a singularity in the limit of neutral stability. The absence of a critical layer for the FSM, owing to its phase speed being (nearly) twice the base-state maximum, implies that $\tilde{\tau}_{xx}$ for this mode exhibits a smooth monotonic variation with z. A comparison of the $\tilde{\tau}_{xz}$ eigenfunctions for both modes again highlights the non-monotonic variation for the CM.

Figures. 11a–c show the CM neutral stability curves in the W–k plane for fixed β and Σ, respectively. For finite Σ and $1-\beta$, these curves are in the form of loops, with the unstable region corresponding to the loop interior, and therefore, being finite in extent; in Fig. 11c, the loops evidently recede upward to infinity for $\beta \to 1$. As discussed earlier, the film-flow CM approaches the channel-flow one for $\Sigma \to \infty$, and this approach is reflected in the changing character of the neutral loops, with increasing Σ, in Fig 11b. While the lower boundary of the neutral loop recedes upward with increasing Σ, corresponding to an increase in the threshold W, there is a concomitant increase in the size of the loops. Eventually, for sufficiently large Σ, this increase in size is primarily an increase in length on account of the the upper boundary receding to infinity, and the lower boundary asymptoting to that for channel flow. Clearly, the infinite-Σ limit is a singular one. For any finite Σ, one has instability only within a neutral loop, implying that there exists a maximum W beyond which the film-flow configuration is stable to perturbations of all wavenumbers. In contrast, the half-channel configuration, that the film-flow stability problem asymptotes to for $\Sigma \to \infty$, has unstable regions that, for any β, appear as infinite-length tongues in the W–k plane that extend all the way to $k = 0$; the upper and lower branches of the tongue following a $W \propto 1/k$ scaling in the small-k limit[30]. In the above sense, the role of surface tension appears to be analogous to that known for finite extensibility in the context of curvilinear shearing flows[11]. In light of the above,

one expects the neutral loops shown in Fig 11b to also morph into tongues for sufficiently large values of Σ, with these tongues now receding to infinity for $\beta \to 1$. When Σ or β varies in the opposite direction, the region of instability shrinks and for sufficiently small Σ's (less than about 4), or for $\beta \lesssim 0.99$, the neutral loop collapses to a point, with the instability being absent for smaller Σ or β. For the range of parameters explored in Fig 11, the critical wavenumber corresponding to the minimum W remains of order unity during this limiting process.

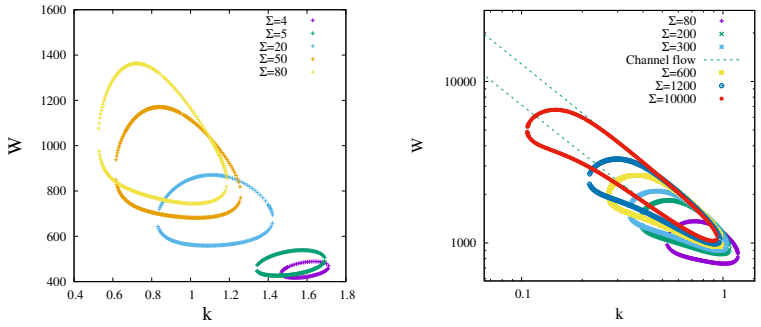

(a) $\beta = 0.995$ for $4 \le \Sigma \le 80$

(b) $\beta = 0.995$ for different $80 \le \Sigma \le \infty$

(c) $\Sigma = 80$ for different β

FIG. 11. Neutral stability curves in the W–k plane, for the elastic centermode, for different Σ (panels (a) and (b)) and different near-unity β (panel (c)); $Re = 0$, $\theta = 50^\circ$. The neutral curves for the channel-flow configuration, corresponding to $\Sigma = \infty$, appear as dashed lines in (b).

The neutral curve for the FSM is shown in Fig 12a. It has a lower branch which asymptotes to a constant W for $k \to 0$, with this lower threshold value agreeing with the results of earlier small-k asymptotic analyses[14,16,47]; the upper branch diverges as $W \propto 1/k$ for $k \to 0$. Note that the finite-W

threshold for the FSM arises due to the choice of inclination ($\theta = 50^\circ$). For the vertical film-flow configuration ($\theta = 90^\circ$) shown in the next figure, instability must arise for any nonzero W or Σ provided k is sufficiently small. In stark contrast to the effect of Σ on the centermode neutral curves in Fig 11a, the neutral curve in Fig 12a, owing to its restriction to very small k's ($k \sim 10^{-3}$ or smaller), is virtually unaffected by Σ. Fig 12b depicts the neutral curves for both the elastic free-surface and center modes on the W–k plane. While the neutral curves for the latter appear smaller in extent owing to the choice of a logarithmic scale, the threshold for the elastic CM is nevertheless higher for the chosen angle of inclination. In the conclusions section, we show that this is no longer the case for sufficiently small θ.

While all of the above results are for an angle of inclination of $\theta = 50^\circ$, in Fig. 13, we show the neutral curve for the vertical film-flow configuration corresponding to $\theta = 90^\circ$. It is known that the FSM in this case is unconditionally unstable for $k \to 0$[16,47], and therefore that there is no longer a lower threshold in the W–k plane. Accordingly, the lower boundary of the envelope turns around and extends vertically down to a critical k that serves as the upper bound for the unstable range of wavenumbers in the limit $W \to 0$. In contrast, the neutral curve for the CM remains qualitatively similar to those for $\theta = 50^\circ$, the implication being that the threshold W for the centermode remains high, within the Oldroyd-B framework, regardless of θ.

Finally, Fig 14 shows the variation of the critical Weissenberg number (W_c, the minimum of the W–k neutral curves) with $(1-\beta)$ for both elastic modes identified, for $\theta = 50^\circ$. The plots show the expected divergence of W_c for $\beta \to 1$. Although the centermode instability also ceases to exist for $\beta \lesssim 0.99$ ($1-\beta \gtrsim 0.01$), akin to the channel flow scenario[30], this transition to stability does not occur via a divergence of W_c for $\beta \to 0.99^+$ (as for channel flow). The difference in behavior is on account of the different shapes of the neutral curves - loops (film-flow for finite Σ) vs tongues (channel flow) in the W–k plane. As already seen in Fig. 11b, the loops simply shrink in size with decreasing β, disappearing for $\beta \lesssim 0.99$. This, in turn, leads to the W_c-curves in Fig. 14 simply terminating in a point at the threshold β. The threshold W for the FSM can be obtained from a low-wavenumber analysis[16] as $W_c = \cot\theta/(2(1-\beta))$ for $\beta \in [0,1)$. An important implication of this expression, which we return to briefly in the conclusions section, is the divergence of the FSM W_c for $\theta \to 0$, which leads to the elastic centermode controlling the transition from the unidirectional laminar state for sufficiently small angles of inclination.

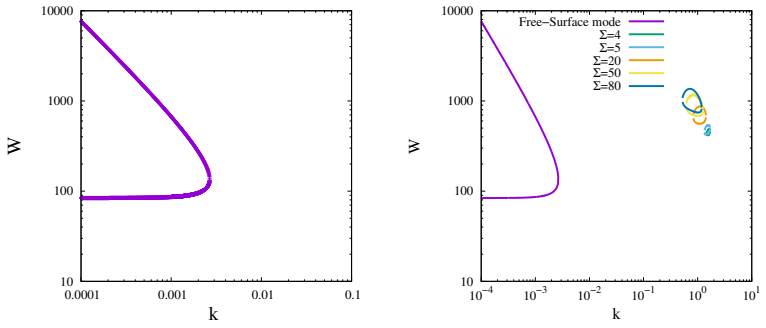

(a) Neutral curve for FSM

(b) Neutral curves for both FSM and cenermodes.

FIG. 12. Neutral stability curve in the W–k plane for the free-surface mode (FSM) (panel (a)) and for both the FSM and centermodes at different Σ's (panel (b)). The neutral curves for the FSM are unaffected by Σ as the instability exists only for low k; $\beta = 0.995$, $Re = 0$, $\theta = 50^\circ$.

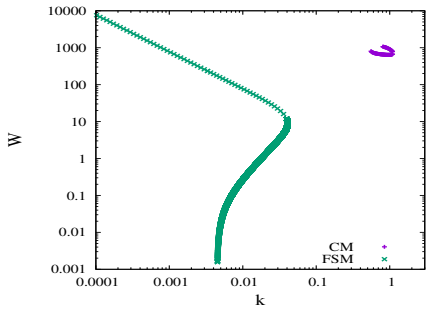

FIG. 13. Neutral curves for both FSM and centermode in the W–k plane for the vertical flow configuration with $\theta = 90^\circ$; Data for $\beta = 0.994$, $\Sigma = 80$, and $Re = 0$.

B. Role of inertia: $Re \neq 0$

In this section, we examine the role of fluid inertia on the centermode and FSM. We characterize inertia using the elasticity number $E = W/Re$. The inertialess limit considered in the previous section corresponds therefore to $E \to \infty$, and we consider here the implications of decreasing E. Inertia is a prerequisite for instability of the FSM in Newtonian film flow[2,3]. With the inclusion of viscoelasticity, the analytical expression for the growth rate in the long-wave limit[16,47] has inde-

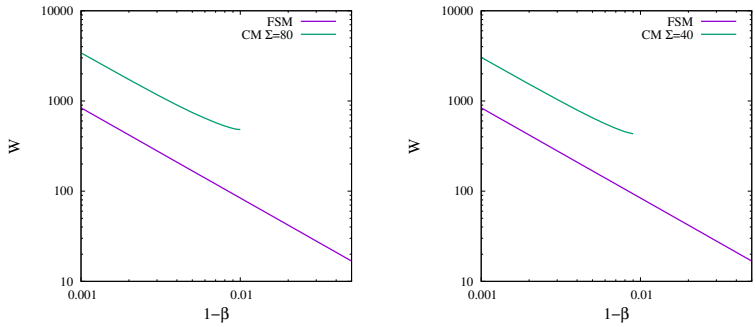

(a) Σ = 80 (b) Σ = 40

FIG. 14. W_c vs (1-β) for the centermode (CM) and free-surface (FSM) instabilities. The centermode instability is absent beyond a threshold $(1-\beta)$, and is affected by Σ. The FSM extends all the way from $0 \leq \beta < 1$ and is independent of Σ; Data for $Re = 0$, $\theta = 50^\circ$.

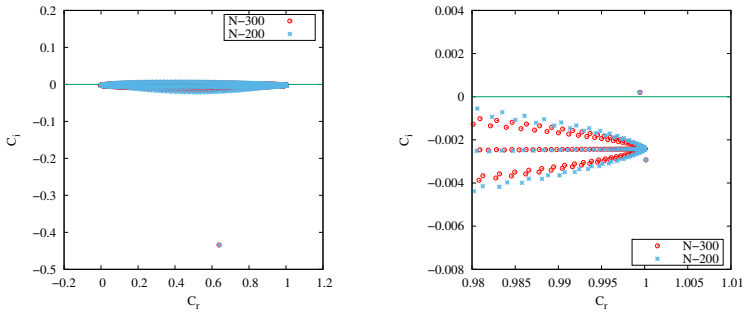

(a) Full Eigenspectrum (b) Zoomed-in view in the neighborhood of $c_r = 1$

FIG. 15. Elastoinertial eigenspectrum for film-flow of an Oldroyd-B fluid with an unstable centermode; $\beta = 0.99$, $k = 0.8$, $Re = 8$, $E = 65$, $\theta = 50^\circ$.

pendent destabilizing contributions from elasticity (proportional to W) and inertia (proportional to Re). Thus, one expects decreasing E to destabilize the FSM, and this expectation will be borne out below. Our earlier investigations of the elastoinertial centermode, especially for channel flow[11,25], has shown that the effect of inertia is rather complicated in this case. For $\beta < \beta_c\,(\approx 0.99)$, inertia has a stabilizing effect with the threshold W increasing as $Re^{\frac{1}{3}}$ (see, for instance, Fig 11a

Accepted to Phys. Fluids 10.1063/5.0154768

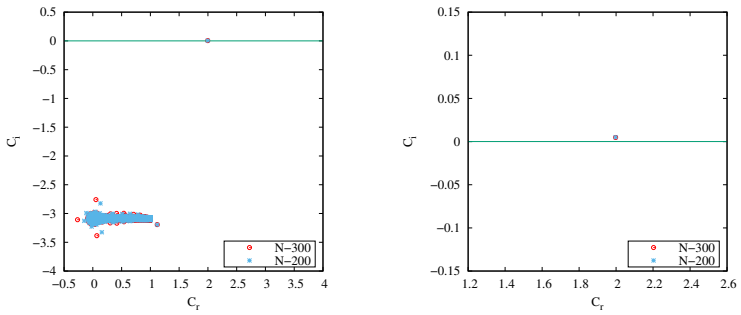

(a) Full Eigenspectrum

(b) Zoomed-in view in the neighborhood of $c_r = 2$

FIG. 16. Elastoinertial eigenspectrum for film-flow of an Oldroyd-B fluid with an unstable FSM; $\beta = 0.99$, $k = 0.001$, $Re = 5$, $E = 65$, $\theta = 50^\circ$.

in Sanchez *et al.* (2022)[11]); on the other hand, for $\beta > \beta_c$, which is when the elastoinertial centermode continues down to $Re = 0$ (morphing into a purely elastic centermode in the process), inertia has an initial destabilizing influence, with W decreasing until a certain Re, before eventually starting to increase as $Re^{\frac{1}{3}}$ (see Fig 11b in Sanchez *et al.* (2022)[11]). Herein, over the range of β and Re examined, we find inertia to have a uniformly destabilizing influence on the film-flow configuration.

To begin with, we show a pair of finite-E spectra, one with an unstable centermode with $c_r \approx 1$ (Fig 15), and the other with an unstable FSM with $c_r \approx 2$ (Fig 16); the second spectrum corresponding to a much smaller value of k. On the whole, these spectra are very similar to their inertialess analogs shown in Figs 2 and 3. In Fig. 17, the dual effect of surface tension Σ, on the elastoinertial centermode, is seen to be analogous to that already seen for the elastic centermode in Fig. 4, with there being an instability only for a finite interval of Σ values. As for the purely elastic case, the stability of the elastoinertial centermode, for both $\Sigma \to 0$ and $\Sigma \to \infty$, is due to the modest value of W. For a higher W, similar to Fig. 5, one finds that the elastoinertial CM remains unstable in the limit $\Sigma \to \infty$; in fact, the threshold W required for the persistence of the CM instability in the infinite-Σ limit is lower on account of the aforesaid destabilizing effect of inertia. The stability of the elastoinertial *CM* in the zero-Σ limit is in contrast to the Newtonian scenario wherein the shear mode remains unstable, for $\Sigma = 0$, over a substantial range of Re[17,18].

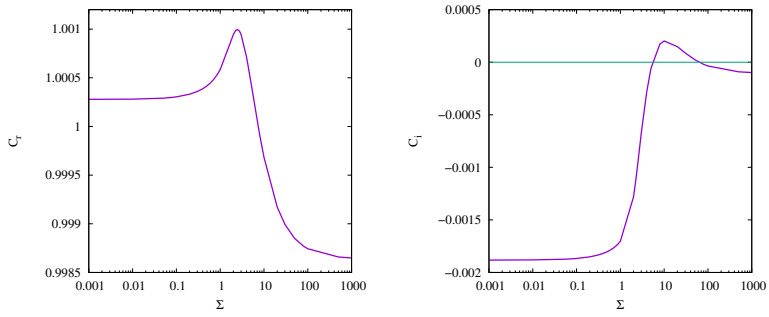

(a) c_r vs Σ (b) c_i vs Σ

FIG. 17. The dual role of surface tension on the elastoinertial centermode, illustrated via the variation of cr and ci as a function of Σ; $\beta = 0.99$, $k = 1.5$, $E = 25$, $Re = 12.79$, $\theta = 50°$.

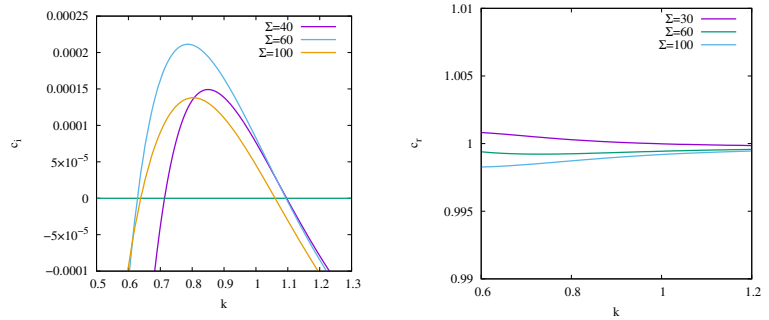

(a) c_i vs. k (b) c_r vs. k

FIG. 18. Variation of c_r and c_i with k for the elastoinertial centermode; $\beta = 0.99$, $E = 65$, $Re = 7.1$, $\theta = 50°$.

The variation of c_r and c_i with k (Fig. 18) shows that the CM instability is present only over a finite range of $O(1)$ k's, similar to the inertialess limit discussed earlier (see Fig. 6). The non-monotonic variation of c_i with Σ, discussed above, is also evident from these figures. In contrast, the variation of c_r and c_i for the FSM (Fig. 19) shows a substantial difference between the inertialess and finite-Re scenarios. The FSM for finite Re's, remains unstable over a much larger range of k's compared to the inertialess limit; the larger k's also lead to a perceptible effect of Σ on both c_r and c_i. As already alluded to at the beginning of the section, this trend can be attributed to the destabilizing role played by fluid inertia via the mechanism already present in Newtonian film flow[2,3].

Accepted to Phys. Fluids 10.1063/5.0154768

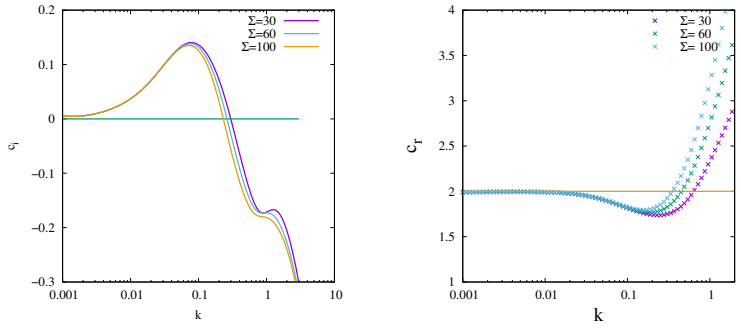

(a) c_i vs. k (b) c_r vs. k

FIG. 19. Variation of c_r and c_i with k for the elastoinertial free-surface mode; $\beta = 0.99$, $E = 65$, $Re = 15$, $\theta = 50°$.

Next, we discuss the neutral stability curves in the W–k and Re–k planes for fixed β and varying E for two different Σ's (Fig. 20). For $\Sigma = 100$, while the unstable loops in the W–k plane shrink in size as E is increased, they eventually asymptote to a finite region in the limit $E \gg 1$ (Fig. 20(a)), implying that the instability continues all the way down to the inertialess limit. This is also seen in the neutral loops in the Re–k plane (Fig. 20(b)); the horizontal extent of these loops remains invariant for $E \to \infty$, corresponding to the unstable range of k in the elastic limit, with their vertical extent decreasing as E^{-1}. In contrast, for $\Sigma = 60$ (Fig. 21), the neutral curves in the W–k plane

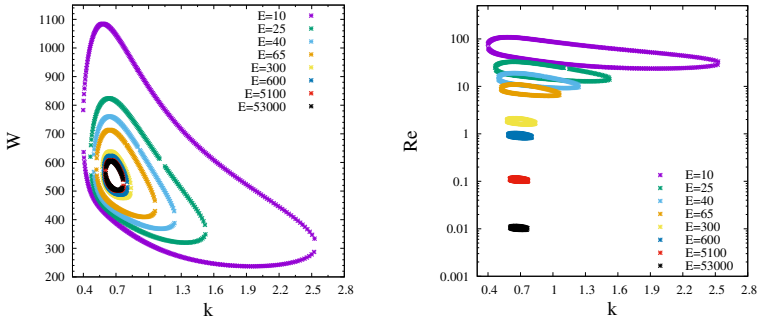

(a) W-k plane (b) Re-k plane

FIG. 20. Neutral stability curves for the elastoinertial centermode in viscoelastic film flow for different E; $\beta = 0.99$, $\Sigma = 100$, $\theta = 50°$. The centermode instability persists in the inertialess limit ($E \to \infty$).

continue to shrink as E is increased, eventually disappearing at a large but finite E (Fig. 21(a)), implying the absence of elastic centermode instability in the inertialess limit for $\Sigma = 60$. A similar trend is seen in the Re–k plane in Fig. 21(b), where the unstable zone shrinks and eventually disappears at a small but finite Re.

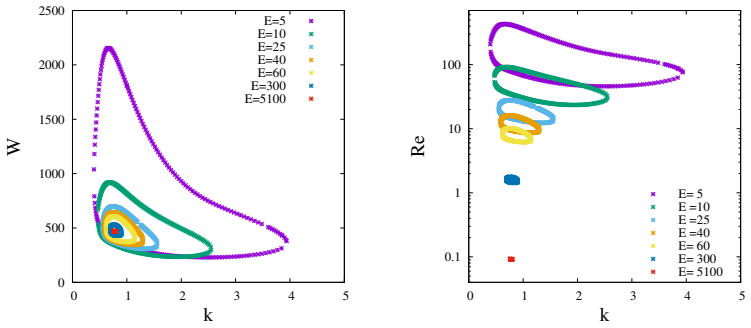

(a) W-k plane (b) Re-k plane

FIG. 21. Neutral stability curves corresponding to the elastoinertial centermode in viscoelastic film flow for different E; $\beta = 0.99, \Sigma = 60, \theta = 50^\circ$. The centermode instability does not continue to the inertialess limit ($E \to \infty$).

In Fig. 22 we show both the neutral curves and phase speeds as a function of E, for the elastoinertial FSM, in the W–k plane. For very large E's, the neutral curve corresponds to the inertialess limit seen earlier in Fig. 12. However, as E is decreased, the range of k's for which the instability persists increases considerably, as already seen in Fig.19. It is useful to define k_{min} as the wavenumber where the W–k neutral curve has a minimum; the neutral curves for the elastoinertial CM shown in Figs. 20 and 21 have a well-defined $k_{min} \sim O(1)$. For the FSM, in contrast, k_{min} is strictly zero (Fig. 22). Thus, in order to quantify the k's where this instability can be observed, it is appropriate instead to use the maximum value of k (referred to as k_{max}) beyond which the FSM is absent in the W–k plane. The variation of k_{max} (for the FSM) and k_{min} (for the CM) with E (Fig. 23) shows that for the FSM, there is a sharp decrease in k_{max} (to $O(10^{-2})$ and smaller) around $E \approx 100$, corresponding to the transition of the neutral curve from a two-lobed to a single-lobed structure. This transition also implies that the FSM for E's of this order or smaller will not be readily realized in experiments, unless configurations, with a sufficiently large extent along the flow direction, are considered. The k_{min} for the centermode always remains $O(1)$ over a wide range of

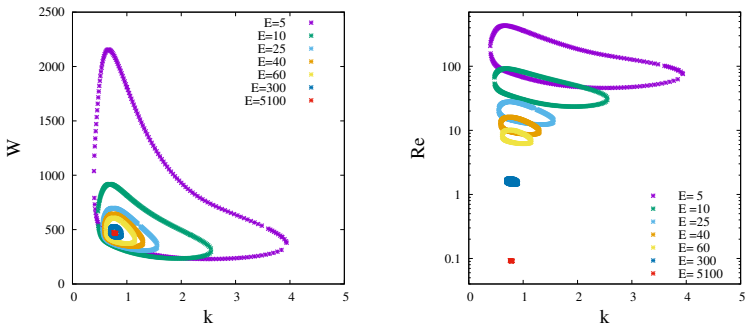

(a) Neutral stability curves in the W–k plane (b) c_r vs k along the neutral stability curve

FIG. 22. Neutral stability curves for the free-surface mode in the W-k plane and the corresponding variation of c_r. Data for $\beta = 0.99, \Sigma = 100$ $\theta = 50°$.

E.

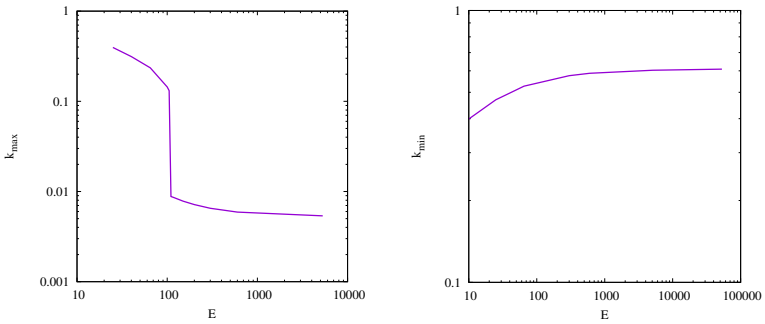

(a) k_{max} vs. E (b) k_{min} vs. E

FIG. 23. Effect of E on k_{max}, the maximum wavenumber up to which the free-surface instability exists in Fig. 22, and k_{min}, the wavenumber at which the minimum occurs in the Re-k neutral curve for the centermode instability in Fig. 20. Data for $\beta = 0.99, \Sigma = 100, \theta = 50°$.

In Fig. 24, we show the variation of Re_c with E for both the center and free-surface modes. For the Σ and β values considered here, both the FSM and centermode continue down to the inertialess limit ($E \to \infty$). This is reflected in the scaling $Re \sim E^{-1}$, seen for $E \gg 1$, for both modes. For finite E, the scaling exponent is weaker than -1, this being consistent with the destabilizing role of inertia alluded to at the beginning of this section. The Re_c for the centermode is consistently

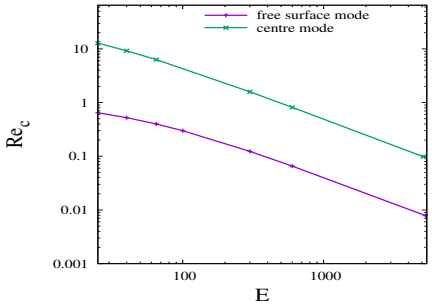

FIG. 24. Variation of Re_c with E for the center and free-surface modes in viscoelastic film flow. Data for $\beta = 0.99$, $\Sigma = 100$, and $\theta = 50^\circ$.

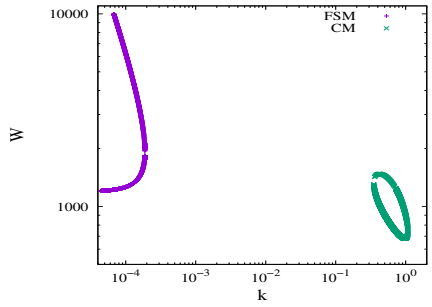

FIG. 25. Neutral curves for both FSM and centermode in the W–k plane for $\theta = 4^\circ$; Data for $\beta = 0.994$, $\Sigma = 80$, and $Re = 0$. For such small angles of inclination, the threshold W for the centermode is lower than that of the FSM.

larger than that for FSM for the entire range of E's shown. However, the feasibility of experimental observation of the CM is nevertheless more favorable compared to the FSM for reasons discussed in the following section.

IV. CONCLUSIONS

We have provided a comprehensive description of the first instance of occurrence of two qualitatively distinct purely elastic instabilities in a given flow configuration - that of gravity-driven viscoelastic film flow down an inclined plane - the viscoelastic fluid being modeled using the

Oldroyd-B constitutive equation. While one of these instabilities, corresponding to a free-surface mode, is known from earlier efforts[14,16], the second is an analog of the novel elastic centermode instability recently identified in plane Poiseuille flow[25,30]. In the inertialess limit, it is shown that the FSM is present only for $k \leq O(10^{-2})$, while the centermode instability is present at $k \sim O(1)$, albeit at higher Weissenberg numbers. With the inclusion of inertia, most of the aforementioned features prevail, except for the larger range of wavenumbers over which the FSM is unstable.

In almost all of the results presented here, we have fixed the angle of inclination at a value (50°) intermediate between the horizontal and vertical orientations; the neutral curves alone have been shown for the vertically oriented configuration. Although the CM threshold has been found to be considerably higher than the FSM one for the above cases, this will no longer be true for $\theta \to 0$. Similar to the Newtonian case[18] discussed in the introduction, one expects the threshold W for the CM instability to become independent of θ for $\theta \to 0$, and therefore, to be lower than that for the FSM (which diverges as $\cot\theta \sim \theta^{-1}$ for in the same limit[14,19]) for sufficiently small angles of inclination. To illustrate this feature, Fig. 25 shows both the FSM and CM neutral curves for $\theta = 4^\circ$; here, the threshold W for the FSM is $O(10^3)$, with the instability being present only for $k < 2 \times 10^{-3}$. In contrast, the threshold W for the CM is much lower (≈ 700), and the critical wavenumber is $O(1)$. It is worth noting that this transition from an FSM-controlled instability to a shear-mode-controlled one occurs at much lower angles of inclination ($\theta \approx 0.5'$) in the Newtonian case.

Moreover, based on recent work on viscoelastic channel flow using the more realistic FENE-P model[28] that incorporates the finite extensibility of the polymer chains, and especially considering the possibility of subcritical bifurcations from the linear threshold, one expects the CM identified here to become more relevant; for instance, in the sense of the CM threshold being lower than the FSM one over a larger range of inclination angles than that found here within the Oldroyd-B framework. We anticipate the predictions in this manuscript to be relevant to viscoelastic coating flows, in terms of aiding the identification of stable operating regimes.

Data Availability: The data that supports the findings of this study are available within the article [and its supplementary material].

REFERENCES

[1]K. J. Ruschak, "Coating flows," Annual Reviews of Fluid Mechanics **36**, 20–53 (2004).

[2]T. B. Benjamin, "Wave formation in laminar flow down an inclined plane," Journal of Fluid Mechanics **2**, 554–573 (1957).

[3]C. Yih, "Stability of liquid flow down an inclined plane," The Physics of Fluids **6**, 321–334 (1963).

[4]C. S. Yih, "Instability due to viscosity stratification," Journal of Fluid Mechanics **27**, 337–352 (1967).

[5]E. J. Hinch, "A note on the mechanism of the instability at the interface between two shearing fluids," Journal of Fluid Mechanics **144**, 463–465 (1984).

[6]Y. Y. Renardy, "Stability of the interface in two-layer Couette flow of upper convected Maxwell liquids," Journal of Non-Newtonian Fluid Mechanics **28**, 99–115 (1988).

[7]K. P. Chen, "Elastic instability of the interface in Couette flow of viscoelastic liquids," Journal of Non-Newtonian Fluid Mechanics **40**, 261–267 (1991).

[8]E. J. Hinch, O. J. Harris, and J. M. Rallison, "The instability mechanism for two elastic liquids being co-extruded," Journal of Non-Newtonian Fluid Mechanics **43**, 311–324 (1992).

[9]J. F. Brady and I. C. Carpen, "Second normal stress jump instability in non-newtonian fluids," Journal of Non-Newtonian Fluid Mechanics **102**, 219–232 (2002).

[10]R. G. Larson, "Instabilities in viscoelastic flows," Rheol. Acta **31**, 213–263 (1992).

[11]H. A. Castillo Sánchez, M. R. Jovanović, S. Kumar, A. Morozov, V. Shankar, G. Subramanian, and H. J. Wilson, "Understanding viscoelastic flow instabilities: Oldroyd-b and beyond," Journal of Non-Newtonian Fluid Mechanics **302**, 104742 (2022).

[12]S. S. Datta, A. M. Ardekani, P. E. Arratia, A. N. Beris, I. Bischofberger, G. H. McKinley, J. G. Eggers, J. E. López-Aguilar, S. M. Fielding, A. Frishman, M. D. Graham, J. S. Guasto, S. J. Haward, A. Q. Shen, S. Hormozi, A. Morozov, R. J. Poole, V. Shankar, E. S. G. Shaqfeh, H. Stark, V. Steinberg, G. Subramanian, and H. A. Stone, "Perspectives on viscoelastic flow instabilities and elastic turbulence," Phys. Rev. Fluids **7**, 080701 (2022).

[13]E. S. G. Shaqfeh, "Purely elastic instabilities in viscometric flows," Annu. Rev. Fluid Mech. **28**, 129–185 (1996).

[14]A. S. Gupta, "Stability of a visco-elastic liquid film flowing down an inclined plane," Journal of Fluid Mechanics **28**, 17–28 (1967).

[15]W. Lai, "Stability of an elastico-viscous liquid film flowing down an inclined plane," The Physics of Fluids **10**, 844–847 (1967), https://aip.scitation.org/doi/pdf/10.1063/1.1762198.

[16]E. S. Shaqfeh, R. G. Larson, and G. H. Fredrickson, "The stability of gravity driven viscoelastic

film-flow at low to moderate reynolds number," Journal of Non-Newtonian Fluid Mechanics **31**, 87–113 (1989).

[17]S. P. Lin, "Instability of a liquid film flowing down an inclined plane," The Physics of Fluids **10**, 308–313 (1967).

[18]J. M. Floryan, S. H. Davis, and R. E. Kelly, "Instabilities of a liquid film flowing down a slightly inclined plane," The Physics of Fluids **30**, 983–989 (1987).

[19]E. Shaqfeh, R. Larson, and G. Fredrickson, "The stability of gravity driven viscoelastic film-flow at low to moderate reynolds number," Journal of Non-Newtonian Fluid Mechanics **31**, 87–113 (1989).

[20]D. Samanta, Y. Dubief, M. Holzner, C. Schäfer, A. N. Morozov, C. Wagner, and B. Hof, "Elasto-inertial turbulence," Proceedings of the National Academy of Sciences **110**, 10557–10562 (2013).

[21]G. H. Choueiri, J. M. Lopez, A. Varshney, S. Sankar, and B. Hof, "Experimental observation of the origin and structure of elastoinertial turbulence," Proceedings of the National Academy of Sciences **118** (2021), 10.1073/pnas.2102350118.

[22]P. Garg, I. Chaudhary, M. Khalid, V. Shankar, and G. Subramanian, "Viscoelastic pipe flow is linearly unstable," Phys. Rev. Lett. **121**, 024502 (2018).

[23]I. Chaudhary, P. Garg, V. Shankar, and G. Subramanian, "Elasto-inertial wall mode instabilities in viscoelastic plane Poiseuille flow," Journal of Fluid Mechanics **881**, 119–163 (2019).

[24]I. Chaudhary, P. Garg, G. Subramanian, and V. Shankar, "Linear instability of viscoelastic pipe flow," Journal of Fluid Mechanics **908**, A11 (2021).

[25]M. Khalid, I. Chaudhary, P. Garg, V. Shankar, and G. Subramanian, "The centre-mode instability of viscoelastic plane poiseuille flow," Journal of Fluid Mechanics **915**, A43 (2021).

[26]M. Dong and M. Zhang, "Asymptotic study of linear instability in a viscoelastic pipe flow," Journal of Fluid Mechanics **935**, A28 (2022).

[27]J. Page, Y. Dubief, and R. R. Kerswell, "Exact travelling wave solutions in viscoelastic channel flow," Phys. Rev. Lett. **125**, 154501 (2020).

[28]G. Buza, J. Page, and R. R. Kerswell, "Weakly nonlinear analysis of the viscoelastic instability in channel flow for finite and vanishing reynolds numbers," Journal of Fluid Mechanics **940**, A11 (2022).

[29]Y. Dubief, J. Page, R. R. Kerswell, V. E. Terrapon, and V. Steinberg, "First coherent structure in elasto-inertial turbulence," Phys. Rev. Fluids **7**, 073301 (2022).

[30]M. Khalid, V. Shankar, and G. Subramanian, "Continuous pathway between the elasto-inertial and elastic turbulent states in viscoelastic channel flow," Phys. Rev. Lett. **127**, 134502 (2021).

[31]H.-H. Wei, "Stability of a viscoelastic falling film with surfactant subjected to an interfacial shear," Phys. Rev. E **71**, 066306 (2005).

[32]S. Pal and A. Samanta, "Linear stability of a contaminated shear-imposed viscoelastic liquid flowing down an inclined plane," Physics of Fluids **33**, 123107 (2021).

[33]S. Pal and A. Samanta, "Linear stability of a surfactant-laden viscoelastic liquid flowing down a slippery inclined plane," Physics of Fluids **33**, 054101 (2021).

[34]T. Hu, Q.-f. Fu, Y. Xing, L.-j. Yang, and L. Xie, "Stability of a thin viscoelastic film falling down an inclined plane," Phys. Rev. Fluids **6**, 083902 (2021).

[35]R. G. Larson, Constitutive Equations for Polymer Melts and Solutions (Butterworths, 1988).

[36]R. B. Bird, R. C. Armstrong, and O. Hassager, Dynamics of Polymeric liquids, Vol 1 Fluid Mechanics (John Wiley, New York, 1977).

[37]Dimensional variables appear with a superscript '$*$' in this work, while dimensionless variables appear without one.

[38]P. G. Drazin and W. H. Reid, Hydrodynamic Stability (Cambridge University Press, 1981).

[39]R. G. Larson, E. S. G. Shaqfeh, and S. J. Muller, "A purely elastic instability in Taylor–Couette flow," Journal of Fluid Mechanics **218**, 573–600 (1990).

[40]Y. L. Joo and E. S. G. Shaqfeh, "Observations of purely elastic instabilities in the taylor–dean flow of a boger fluid," Journal of Fluid Mechanics **262**, 27–73 (1994).

[41]J. A. Byars, A. Oztekin, R. A. Brown, and G. H. McKinley, "Spiral instabilities in the flow of highly elastic fluids between rotating parallel disc," J.Fluid Mech. **271**, 173–218 (1994).

[42]G. H. McKinley, J. A. Byars, R. A. Brown, and R. C. Armstrong, "Observations on the elastic instability in cone-and-plate and parallel-plate flows of a polyisobutylene boger fluid," Journal of Non-Newtonian Fluid Mechanics **40**, 201 – 229 (1991).

[43]P. Pakdel and G. H. McKinley, "Elastic instability and curved streamlines," Phys. Rev. Lett. **77**, 2459–2462 (1996).

[44]H. J. Wilson, M. Renardy, and Y. Y. Renardy, "Structure of the spectrum in zero Reynolds number shear flow of the UCM and Oldroyd-B liquids," Journal of Non-Newtonian Fluid Mechanics **80**, 251–268 (1999).

[45]M. Khalid, I. Chaudhary, P. Garg, V. Shankar, and G. Subramanian, "The centre-mode instability of viscoelastic plane Poiseuille flow," Journal of Fluid Mechanics **915**, A43 (2021).

[46]H. Chang, "Wave evolution on a falling film," Annual Reviews of Fluid Mechanics **26**, 103–136 (1994).

[47]A. Jain and V. Shankar, "Instability suppression in viscoelastic film flows down an inclined plane lined with a deformable solid layer," Physical Review E **76**, 046314 (2007).